PHOTONICS Research

10 Gbps wavelength division multiplexing using UV-A, UV-B, and UV-C micro-LEDs

Daniel M. Maclure,[1,5] Jonathan J. D. McKendry,[1] Mohamed Sufyan Islim,[2] Enyuan Xie,[1] Cheng Chen,[2] Xiaobin Sun,[3] Xudong Liang,[4] Xiaohui Huang,[4] Hanaa Abumarshoud,[2] Johannes Herrnsdorf,[1] Erdan Gu,[1,6] Harald Haas,[2] and Martin D. Dawson[1]

[1]Institute of Photonics, Department of Physics, SUPA, University of Strathclyde, Glasgow G1 1RD, UK
[2]LiFi Research and Development Centre, Department of Electronic & Electrical Engineering, University of Strathclyde, Technology & Innovation Centre, Glasgow G1 1RD, UK
[3]Fraunhofer Center of Applied Photonics, Technology & Innovation Centre, Glasgow G1 1RD, UK
[4]Zhixin Semiconductor (Hangzhou) Co., Ltd., Hangzhou 311200, China
[5]e-mail: daniel.maclure@strath.ac.uk
[6]e-mail: erdan.gu@strath.ac.uk

Received 25 October 2021; revised 8 December 2021; accepted 8 December 2021; posted 13 December 2021 (Doc. ID 445984); published 1 February 2022

Deep ultraviolet (DUV) optical wireless communications have seen increased interest in recent years due to the unique properties of light in this spectral region. However, the reported DUV data rates remain significantly lower than comparable demonstrations at visible wavelengths due to lower modulation bandwidths and/or output power of the sources. Here, we present a wavelength division multiplexing demonstration using three UV micro-light-emitting diodes emitting at nominal peak wavelengths of 285, 317, and 375 nm, respectively, each with an emitting area of approximately 1369 μm^2 (equivalent to circular device pixels of diameter ∼40 μm). Using orthogonal frequency division multiplexing, data rates of 4.17, 3.02, and 3.13 Gbps were achieved from the 285, 317, and 375 nm devices, respectively, for a combined data rate of 10.32 Gbps transmitted over a distance of 0.5 m.

https://doi.org/10.1364/PRJ.445984

1. INTRODUCTION

Optical wireless communication (OWC) has seen much attention as a possible solution to the predicted "data crunch" facing radio frequency (RF) communications [1,2]. The visible and ultraviolet regions of the electromagnetic spectrum are license-free and largely unexploited thus far and, as a result, offer additional frequency bandwidth to complement RF communications.

Ultraviolet (UV) communication is an important emerging area of OWC, as it can be used in a wide range of applications such as secure communications and non-line of sight (NLOS) communications. A significant benefit of operating at deep UV (DUV) wavelengths, i.e., in the UV-B (280–315 nm) or UV-C (100–280 nm) spectral bands, is that sunlight at these wavelengths is absorbed by the upper atmosphere, resulting in an essentially noiseless environment for terrestrial DUV communication [3]. Furthermore, it also benefits secure intersatellite communications, as the space-based ultraviolet signal is obscured from ground observers. UV light is also strongly scattered by air, allowing for NLOS wireless optical communication over/around physical obstacles such as buildings. This is due to the fact that the strength of Rayleigh scattering is inversely proportional to λ^4, where λ is the wavelength of light, and thus short-wavelength UV is much more strongly scattered by air than visible wavelengths. This property can help support NLOS wireless optical communication through the atmosphere, relaxing the constraints on transceiver pointing and tracking, and allowing physical obstacles such as buildings that might block LOS links to be overcome.

UV sources have seen significant improvements recently. Previously, mercury lamps with kHz optical modulation bandwidths were the primary sources available, meaning it was impossible to achieve high data rates. These sources are also bulky and fragile, and contain toxic materials. DUV lasers have also attracted interest due to their high bandwidth and high power [4]. However, their highly directional emission and eye safety requirements [5,6] and challenges in fabricating laser diodes emitting at wavelengths below 315 nm hamper their wide-scale adoption in real-world applications [7]. On the

other hand, with improving semiconductor material quality, output power, and efficiency, UV light-emitting diodes (LEDs) are becoming the source of choice for various applications, including sterilization and UV optical communications.

In this work, we use micrometer scale (<100 μm) LEDs (μLEDs) as optical transmitters. Such μLEDs have witnessed a surge of interest with recent developments such as high-resolution displays [8] and visible light applications [9,10]. The main benefit of μLEDs for optical communications, when compared with conventional large area LEDs, is their high bandwidth. Due to their small size, μLED capacitance is small; hence, their bandwidth is limited by the carrier lifetimes rather than a large RC time constant as in conventional LEDs [11]. This allows for faster modulation, with bandwidths in excess of 650 MHz being reported [12], compared with around 10 MHz for a conventional LED. Data rates achieved from single visible-emitting μLEDs have approached 10 Gbps [12]; however, corresponding rates from UV μLEDs have thus far been limited to around 2 Gbps [13], primarily due to the comparatively low output powers at these wavelengths.

This paper demonstrates wavelength division multiplexing (WDM) using three UV μLEDs with peak emission at 285, 317, and 375 nm, respectively. WDM allows optical data to be encoded separately in different wavelength bands and transmitted in parallel to increase throughput. Using orthogonal frequency division multiplexing (OFDM) and quadrature amplitude modulation (QAM) encoding, data rates of 4.17, 3.02, and 3.13 Gbps from the 285, 317, and 375 nm μLEDs, respectively, were demonstrated, giving a total aggregate data rate of 10.32 Gbps transmitted over 0.5 m. This, to the best of our knowledge, is the highest data rate yet reported using UV LEDs and for the first time that WDM has been used for OWC across the UV spectrum.

2. μLED DEVICES

In this work, three μLED arrays with peak emission wavelengths within the UV-C (285 nm), UV-B (317 nm), and UV-A (375 nm) regions of the spectrum were fabricated from commercial-grade III-nitride LED wafers grown on 2 in. *c*-plane sapphire substrates. Details of the wafer structures for the UV-C and UV-A devices can be found in our previous work [14–16].

The UV-B wafer was custom fabricated for this work by Zhixin Semiconductor Co., Ltd. on a 2 in. sapphire substrate. The wafer contained a 2000 nm thick AlN buffer, a 1000 nm thick undoped AlGaN layer, and two 500 nm n-doped layers of AlGaN:Si with Al concentrations of 50% and 55%, respectively. The active region contained a multiple quantum well (MQW) region and consisted of AlGaN with Al concentration of 15%/40%, a 50 nm thick electron blocking layer (EBL) of AlGaN:Mg with Al composition of 50%, and, finally, a 300 nm p-doped region of GaN:Mg and a 10 nm thick GaN:Mg p-contact region.

The design and fabrication process of these μLED arrays were similar to those reported in our previous work [17]. As shown in Fig. 1, each array consists of eight trapezoidal-shaped μLED pixels in a flip-chip configuration, with each pixel having an emission area of 1369 μm^2, an area equivalent to a circular disk-shaped pixel of ∼40 μm diameter. The trapezoidal-shaped pixels were first reported in Ref. [17], where it was speculated that the shape increased the surface-to-active-area ratio, thus enabling a more efficient thermal dissipation. The fabricated arrays were then wire-bonded to a printed circuit board for further characterization.

The light output power versus current (*L-I*) and current versus voltage (*I-V*) relationships were measured from representative pixels from each device. The *I-V* characteristics were measured using a Yokogawa GS610 source measure unit, and the *L-I* characteristics were measured by placing the pixels in close proximity to a calibrated Thorlabs S120VC power meter head. The results are shown in Fig. 2.

The maximum output powers per pixel are approximately 0.48, 0.14, and 1.32 mW for the UV-C, UV-B, and UV-A devices, respectively. The most efficient device was the UV-A, which was expected, as this material technology is the most mature, and issues such as defects are minimized. The relatively low output power of the UV-B device may be attributed to the relative lack of development of material at these wavelengths, as there is currently no high-volume application for LEDs emitting in this range [18].

The forward voltages at 10 mA were 18.4, 22.0, and 4.4 V for the UV-C, UV-B, and UV-A devices, respectively. The

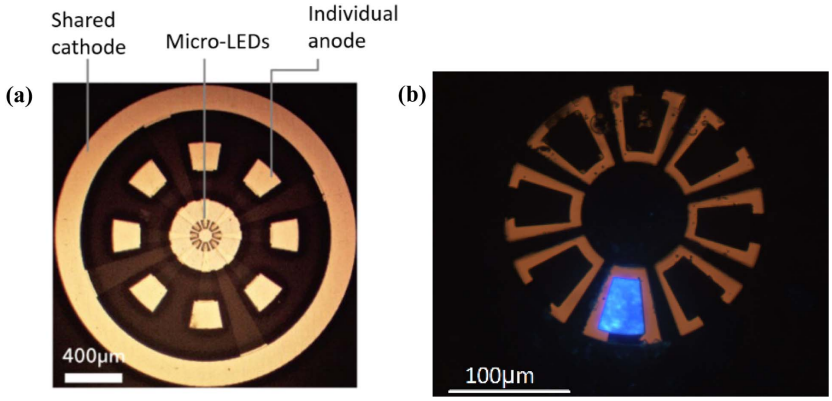

Fig. 1. (a) Top-down micrograph image representation of a micro-LED array, showing the eight concentric and individually addressable pixels. (b) UV-C pixel in operation.

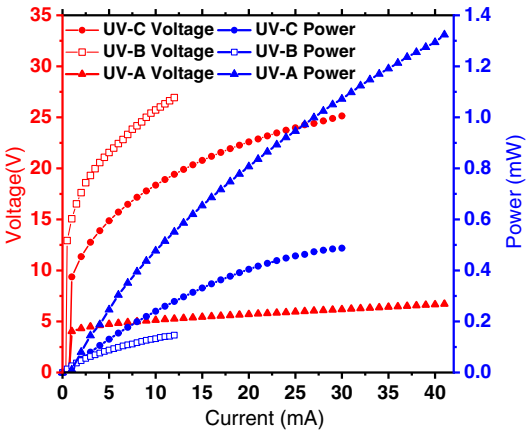

Fig. 2. *L-I-V* curves of the devices at UV-A, UV-B, and UV-C wavelengths.

higher turn-on voltages for the UV-B and UV-C devices can be attributed to the poor electrical conductivity of AlGaN layers, resulting in inferior carrier injection [18] and difficulties in creating low-resistance Ohmic contacts at higher Al mole fractions. These are prevalent issues in DUV material, and devices with higher turn-on voltages also being reported in the literature [5,19].

The EL spectra of the devices as a function of current were measured using a spectrometer and fiber optic (Avantes Avaspec-20482 spectrometer and Ocean Optics QP600-2-SR-BX fiber) (see Fig. 3). The peak wavelengths for each device were measured to be 281.7, 316.5, and 373.4 nm, respectively, when operating at 10 mA.

The spectra of the devices demonstrated different redshifts with the increasing current. This suggests heating effects were a more prominent issue in the UV-C device, which demonstrated a shift in the peak wavelength of 3.5 nm (from 281.7 to 285.2 nm) with increasing current from 0 to 30 mA. The shift is not as prominent in the other devices, with shifts of 1.2 nm being recorded for the UV-B over a current range of 0–12 mA and 1.16 nm being recorded in the UV-A devices, over the same range of current as the UV-C device. The measured spectra helped inform what filters and mirrors would be used in the WDM setup, which will be discussed in Section 3. It was noted that there was spectral overlap between

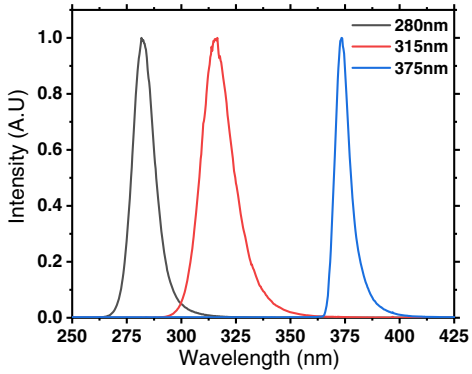

Fig. 3. EL spectra of the three devices at 10 mA.

the UV-C and UV-B devices, which could result in a degree of crosstalk between these WDM channels.

Finally, the frequency responses of the devices were measured using an avalanche photodiode (APD, Hamamatsu C5668 8867) with a bandwidth range of 100 kHz to 1 GHz, following a similar procedure, as outlined in our previous work [16]. Values for each device's −3 dB electrical-to-electrical (E-E) bandwidths were obtained from the recorded frequency responses as a function of current.

Conventionally, when plotted on a logarithmic frequency scale, the frequency response of an LED should appear flat at low frequencies before gradually rolling off above a certain cut-off frequency. The −3 dB bandwidths can then simply be obtained by finding the frequency at which the response of the LED is −3 dB lower than the flat low-frequency part of the response curve. However, the UV-B and UV-C devices exhibited frequency response behaviors, which showed the response initially rising to a broad peak, before gradually rolling over, as shown in Fig. 4. This complicates the process of estimating the devices' bandwidths. We tentatively attribute this behavior to the effect of parasitic impedance from wire bonds and packaging and the μLEDs themselves.

Our approach was to arbitrarily set the response at 1 MHz as the low-frequency reference and define the μLED bandwidth as the frequency at which the response declined to −3 dB below this point. This is illustrated in Fig. 4. This allowed the general behavior of μLED bandwidth versus current to be estimated, though it makes a like-for-like comparison of μLED bandwidths reported elsewhere challenging. The resulting E-E bandwidth as a function of current for all devices is shown in Fig. 5.

The corresponding E-E bandwidths were found to be 960, 780, and 140 MHz, respectively. It is worth noting that the APD bandwidth (1 GHz) is close to that of the UV-B and -C μLEDs and, as a consequence, may have affected the estimated bandwidths. The further development of high-bandwidth UV/DUV sensitive APDs is urgently needed to facilitate the full measurement of μLED devices such as those reported here. Compared with their UV-A counterparts, the high modulation bandwidths and lower output power of the UV-B and -C devices

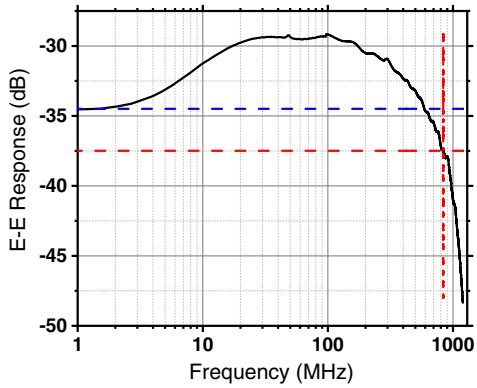

Fig. 4. Frequency response of the UV-C μLED measured at 20 mA (black). The response at 1 MHz (indicated by the blue horizontal dotted line) is used as the low-frequency reference point to estimate the E-E −3 dB bandwidth (indicated by the red crosshair).

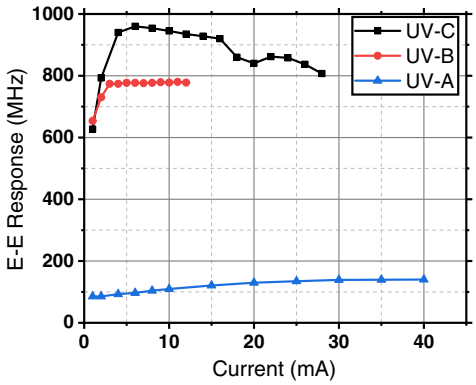

Fig. 5. Electrical-to-electrical bandwidth response versus current for the respective wavelengths.

may be attributed to higher defect densities and thus increased nonradiative recombination at shorter wavelengths. This would lead to lower output power and higher bandwidth via a reduced carrier recombination lifetime. We speculate that the saturation and decrease of the bandwidth as seen in the UV-B and UV-C, respectively, may be attributed to device heating and thermally mediated effects such as carrier overflow reducing the carrier density in the quantum wells, thus increasing the average carrier lifetime and reducing the bandwidth [20].

3. WDM EXPERIMENTAL SETUP

The WDM optical setup consists of the three UV μLED arrays and two long-pass dichroic mirrors with cut-on wavelengths of 355 nm (Semrock Di01-R355-25 × 36) and 300 nm (Alluxa-8113, 300 LP Dichroic). The transmission spectra of these mirrors are shown in Fig. 6, along with the respective device spectra at 10 mA. The mirrors were used to combine the light from the three μLEDs into a common optical path, as seen in Fig. 7. These components were connected in an optomechanical cage system with the arrays mounted on manually adjustable stages to facilitate optimized alignment. The relatively small variation in the μLED emission spectra as a function of current was not found to cause any significant problems in discriminating between channels.

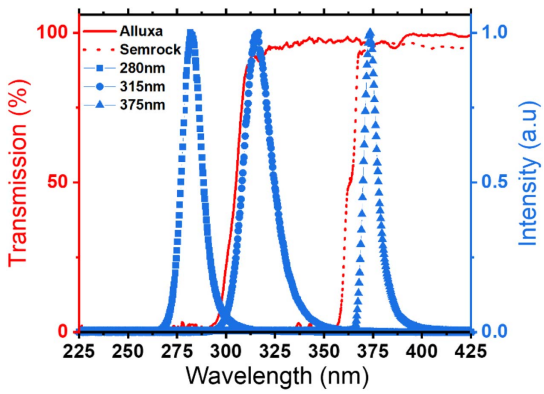

Fig. 6. Spectra (red curves) of the dichroic mirrors used in the setup, and the spectra (blue data points) of the devices with each device operated at 10 mA.

The emission from each μLED array was focused using a separate 2 in. diameter lens [Edmund Eptics 84340, focal length 40 mm for the UV-C and UV-B μLEDs, Thorlabs ACL50832U-A lens (NA = 0.76) for UV-A]. Three bias-TEEs (Tektronix PSPL5675A, a Mini-Circuits ZFBT-4R2G, and Mini-Circuits ZFBT 6GW-FT+) supplied the RF modulation signals and DC power to the pixels. A Keysight M8195A arbitrary waveform generator (AWG), with a peak-to-peak voltage of 250 mV, sampling rate of 65 GSamples/s, analogue bandwidth of 25 GHz, and vertical resolution of 8 bits, was used to provide the modulation signals. Figure 7 shows a schematic of the experimental arrangement.

A MATLAB code was used to generate the DC-biased optical (DCO)-OFDM data similar to our previous work [16,21,22]. This code allowed for the evaluation and control of the setup's performance, such as the peak-to-peak voltage, OFDM signal clipping, modulation bandwidth, number of subcarriers, cyclic prefix (CP) length, and the target bit error rate (BER) for adaptive bit and energy loading algorithm, which determined the final data rates achieved. Before transmitting the OFDM signal, a sinusoidal waveform was used to find an appropriate bias point with suitable peak-to-peak voltage and avoid any severe nonlinear distortion or saturation. After analyzing the performance, the following parameters were used: CP length of 20, normalized clipping level set to 3.2 of the signal standard deviation, corresponding PAPR of 10.1 dB, an FFT size of 2048, and a training length of 1504 QAM OFDM frames.

Next, a channel and signal-to-noise ratio (SNR) estimation procedure is executed, where 4QAM symbols are supplied to all subcarriers as the pilot signals. After an FFT (fast Fourier transform) operation, the detected symbols were compared with the original pilot symbols to estimate the channel gain and SNR for each subcarrier. The SNR information enables the use of an adaptive bit and energy loading algorithm [12], which selects the most suitable QAM constellation and transmission power for each subcarrier so that the eventual achieved BER will converge to a predefined threshold, thus maximizing the achievable data rate.

Next, the payload OFDM signal is transmitted. The QAM constellation and power control on each subcarrier are defined based on the adaptive bit and energy loading result. On the receiver side, the detected frequency-domain symbols are equalized using the estimated channel. Finally, the equalized symbols are decoded and compared with the original binary bits for BER calculation. The BER target used here is 3.8×10^{-3}, as this value allows the use of forwarding error correction codes to provide virtually error-free communication with a 7% overhead.

In the WDM experiment, one μLED at a time was modulated with an OFDM signal, while the code simultaneously generated interfering signals in the other two μLED channels in order to simulate a real-world system with multiple parallel data streams. Furthermore, three amplifiers (one SFHS126A and two Minicircuits FL-1000LN+ amplifiers) were connected between the AWG and the bias TEE to amplify the RF signal

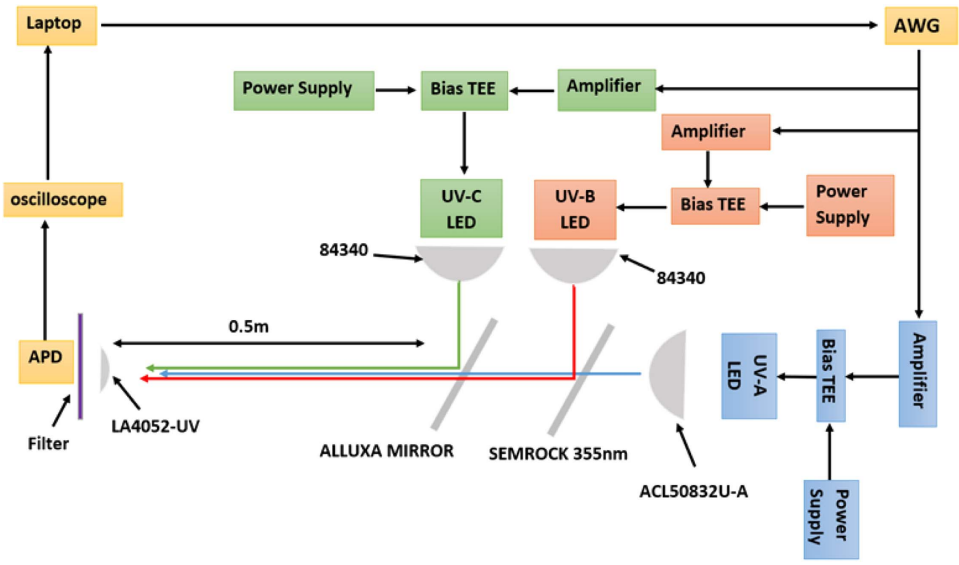

Fig. 7. Schematic diagram of the optical and electrical setup used for the WDM transmission experiments.

and increase the signal modulation depth. The SFHS126A amplifier, with a gain of 29 dB, was connected to the μLED sending the desired OFDM signal. The receiver was situated 0.5 m from the transmitter. According to Ref. [23], the absorption and scattering coefficients at these wavelengths are on the order of 0.1–0.3 km^{-1}, meaning that, at this transmission distance, the absorption and scattering effects can be considered negligible. In particular, this means that there is effectively no difference in scattering of the three selected WDM wavelengths over distances well beyond the tens of meters range. A single 1 in. lens (Thorlabs LA4052, focal length 35.1 mm) was used to focus the received signals onto the receiver. A sliding filter mount (Thorlabs CFS1/M) was used to mount three filters (Semrock FF01 280/20-25, Envin 308 nm bandpass filter, and Edmund Optics 34299 350 nm long-pass filter) and select the channel of interest. Finally, an APD with 1 GHz bandwidth (Hamamatsu C5668 8867) was used as the detector. Only one detector is used in this configuration compared with the multiple detector methods commonly used in this field [24]. This choice was made to simplify the setup. This detector was connected to an oscilloscope (Keysight MXR608A: sampling rate, 16 GSamples/s; analogue bandwidth, 6 GHz; vertical resolution, 10 bits) and a laptop to capture received waveforms for offline processing. From this, it was possible to determine the SNR, bit error rate (BER), and the maximum "error-free" data rates per channel, which will be discussed in the next section.

4. EXPERIMENTAL RESULTS

Before carrying out the main WDM experiment, the effect of the optical setup on the performance of the individual devices was examined. The performance of individual channels was evaluated where only one channel was operating at a time, and the performance was compared with and without a filter in front of the receiver. When filters were applied, a decrease in the SNR of each channel was observed due to optical losses from the filters. The decrease in SNR translated to an increase in the BER and thus a decrease of the maximum data rate.

The BER versus data rate for each channel with and without the corresponding receiver filter is shown in Fig. 8(a). The maximum data rates for the UV-A device were 3.46 and 3.56 Gbps with and without the filter, respectively. The UV-B maximum data rate decreased from 3.4 Gbps without the filter to 3.15 Gbps with the filter; for the UV-C, the corresponding decrease was from 4.52 to 4.17 Gbps. We note that, in multicarrier transmission systems such as what is used here, advanced equalization techniques permit modulation well beyond the 3 dB E-E response of the device, as shown here and demonstrated in other studies [25]. For the full WDM configuration, with all channels active and modulated with one channel transmitting a random bit stream and the other channels generating random noise, the SNR of each of the WDM channels was characterized. The peak-to-peak modulation voltage supplied by the AWG in all cases was 0.25 V. This was amplified, and the corresponding bias current for each μLED is shown in Table 1. As shown in Fig. 8(b), the SNR of the UV-B device is lower than that of the other devices. This was expected, as the power output of this device was notably less than that of the other devices. Furthermore, the SNR of the UV-A channel is degraded by optical crosstalk from the UV-B device. This could be mitigated in the future with improved receiver filters. Figure 8(b) shows that approximately 1.30, 1.10, and 1.25 GHz channel bandwidth was accomplished with an SNR > 5 dB for the UV-C, -B, and -A channels, respectively. The large bandwidth available from each WDM channel allows a substantial number of parallel OFDM subcarriers to be used and maximize the achievable data rates.

M-QAM constellation diagrams from each WDM channel are shown in Fig. 9. As shown, the largest constellation sizes used were 32, 16, and 16 for the UV-C, -B, and -A channels, respectively, with corresponding BERs of 1.12×10^{-4}, 2.40×10^{-4}, and 1.36×10^{-4}. A larger constellation could be

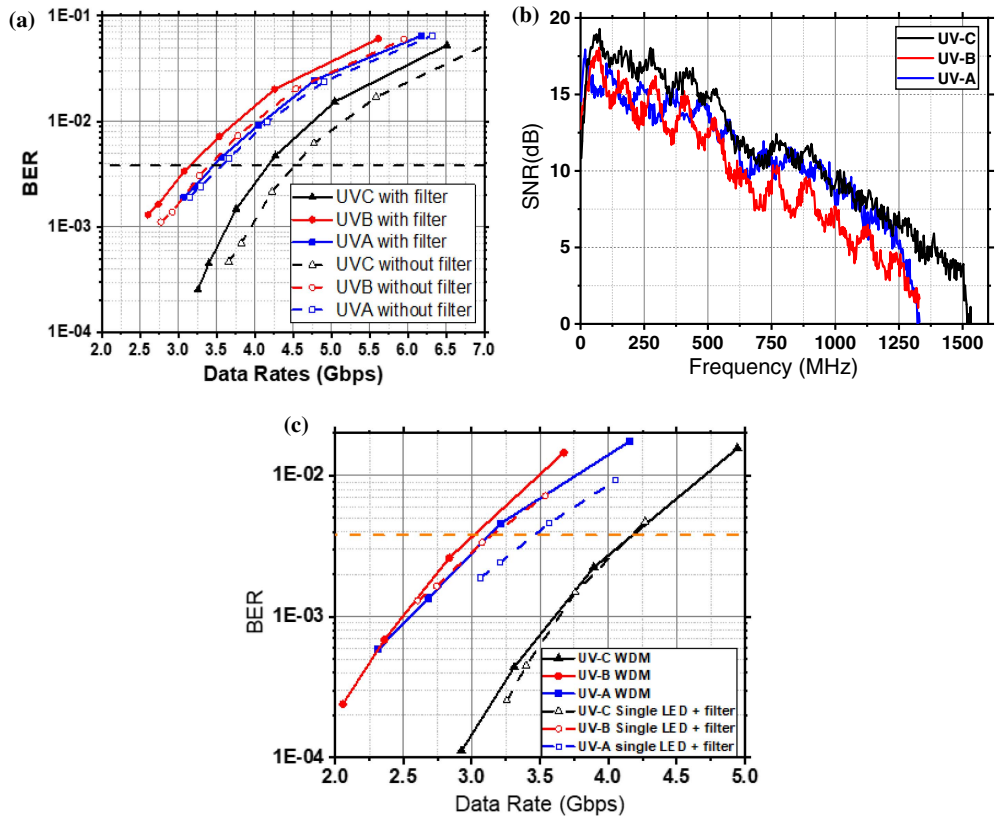

Fig. 8. (a) Comparison of BER when filters are applied to single pixels. (b) SNR of the devices in the WDM setup. (c) BER of three devices in the WDM setup. The dashed horizontal line in (a) and (c) corresponds to a BER of 3.8×10^{-3}.

Table 1. OFDM Parameters and Achieved Data Rates

Device	Operating Current (mA)	Maximum Data Rate (Gbps)
UV-A	30	3.13
UV-B	12	3.02
UV-C	30	4.17
Total		10.32

used on the UV-C channel due to it having higher modulation bandwidth than the UV-A channel and higher output power and SNR than the UV-B device.

The maximum data rates recorded were 4.17, 3.02, and 3.13 Gbps for the UV-C, -B, and -A devices, respectively, as can be seen in Fig. 8(c). The data rates per channel are also given in Table 1, at a BER of approximately 3.8×10^{-3}. The total aggregate WDM data rate achieved was 10.32 Gbps.

The performance of the devices behaved as expected based on the characterization measurements, with the UV-B showing the lowest maximum data rate. As shown in Fig. 2, the UV-B device emits the lowest output power among the three devices shown here. A small fraction of this output power is also lost when combining the three devices' emission together for WDM, due to the less than 100% transmission of the "Alluxa" mirror, as shown in Fig. 6. It also has lower bandwidth than the UV-C device. These factors all contribute to the comparatively low data rate achieved by the UV-B device, even though this device had a higher bandwidth than the UV-A device.

When comparing the BER of the single pixels operating individually with the WDM values, the UV-C device produces similar results in both the WDM and the single device configuration. This can be attributed to the fact that the UV-C experienced the least crosstalk, as the filters and mirrors removed the unwanted light from the UV-B and -A devices. Conversely, the UV-B and UV-A channels show a marked improvement when only one pixel is on. This is due to the spectral overlap resulting in interference from adjacent channels affecting them, which is especially clear in the UV-A channel. The average received powers were estimated using a calibrated optical power meter to be 0.25, 0.03, and 0.10 mW for the UV-A, -B, and -C, respectively. However, due to the difference in active area between the power meter sensor and APD (9 and 0.5 mm diameter, respectively), the actual average received powers are likely to be significantly lower than this.

To the best of our knowledge, the highest optical wireless data rate reported for a single DUV μLED was 2 Gbps obtained by Zhu *et al.* [13] for a UV-C μLED. In the UV-B, Sun *et al.* demonstrated 71 Mbps using an LED [26]. As shown in Table 1, our UV-B and UV-C channels significantly exceed these, and the maximum data rates shown here are, to the best of our knowledge, the highest reported in each of the UV-A, -B, and -C bands. Furthermore, this first demonstration of applying WDM to DUV LEDs allowed the aggregate data rate to

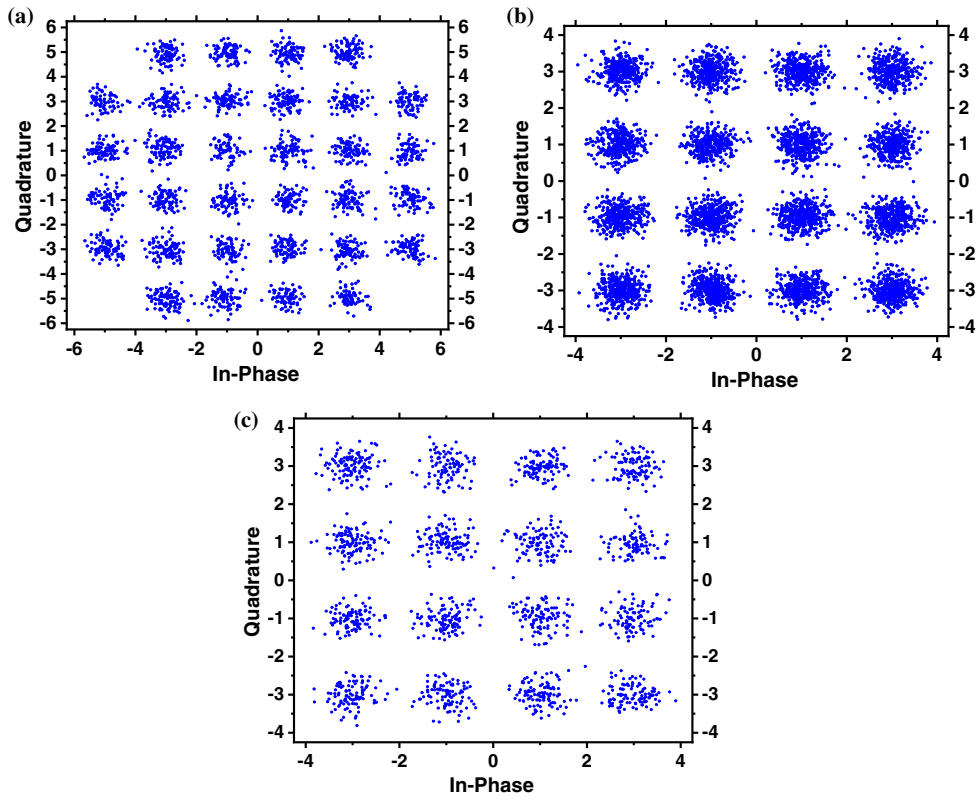

Fig. 9. Maximum *M*-QAM constellation sizes achieved: (a) 32 QAM for UV-C, (b) 16-QAM for UV-B, and (c) 16-QAM for UV-A.

exceed the benchmark of 10 Gbps for the first time using LEDs emitting in the DUV.

5. CONCLUSION

This work has demonstrated a three-channel UV-WDM setup using μLEDs with peak emission in the UV-A (375 nm), UV-B (317 nm), and UV-C (285 nm) regions of the ultraviolet spectrum. Using OFDM and QAM modulation schemes and forward error correction, we achieved data rates of 4.17, 3.02, and 3.13 Gbps from the UV-C, UV-B, and UV-A devices, respectively. The data rates from each individual channel, taken in isolation, represent, to our best knowledge, the highest rates yet reported for a UV μLED and, added together, result in a combined data rate of 10.32 Gbps, demonstrating an LED-based UV optical wireless link exceeding 10 Gbps.

Funding. Engineering and Physical Sciences Research Council (EP/M01326X/1, EP/S001751/1, EP/T00097X/1).

Acknowledgment. We acknowledge Zhixin Semiconductor Co., Ltd. for the LED wafer material. We acknowledge Fraunhofer UK Research Ltd. for DM's PhD studentship funding. All authors declare there are no competing financial interests involved in this work.

Disclosures. The authors declare no conflicts of interest.

Data Availability. The data are available at [27].

REFERENCES

1. H. Haas, "LiFi is a paradigm-shifting 5G technology," Rev. Phys. **3**, 26–31 (2017).
2. D. O'Brien, S. Rajbhandari, and H. Chun, "Transmitter and receiver technologies for optical wireless," Philos. Trans. R. Soc. A **378**, 20190182 (2020).
3. R. J. Drost and B. M. Sadler, "Survey of ultraviolet non-line-of-sight communications," Semicond. Sci. Technol. **29**, 084006 (2014).
4. G. Chen, Z. Xu, and B. M. Sadler, "Experimental demonstration of ultraviolet pulse broadening in short-range non-line-of-sight communication channels," Opt. Express **18**, 10500–10509 (2010).
5. A. Vavoulas, H. G. Sandalidis, N. D. Chatzidiamantis, Z. Xu, and G. K. Karagiannidis, "A survey on ultraviolet C-band (UV-C) communications," Commun. Surveys Tuts. **21**, 2111–2133 (2019).
6. Z. Xu and B. M. Sadler, "Ultraviolet communications: potential and state-of-the-art," IEEE Commun. Mag. **46**, 67–73 (2008).
7. Z. Zhang, M. Kushimoto, T. Sakai, N. Sugiyama, L. Schowalter, C. Sasaoka, and H. Amano, "A 271.8 nm deep-ultraviolet laser diode for room temperature operation," Appl. Phys. Express **12**, 8–12 (2019).
8. H. S. Wasisto, J. D. Prades, J. Gülink, and A. Waag, "Beyond solid-state lighting: miniaturization, hybrid integration, and applications of GaN nano-and micro-LEDs," Appl. Phys. Rev. **6**, 041315 (2019).
9. G.-R. Lin, H.-C. Kuo, C.-H. Cheng, Y.-C. Wu, Y.-M. Huang, F.-J. Liou, and Y.-C. Lee, "Ultrafast 2 × 2 green micro-LED array for optical wireless communication beyond 5 Gbit/s," Photon. Res. **9**, 2077–2087 (2021).
10. D. Peng, K. Zhang, and Z. Liu, "Design and fabrication of fine-pitch pixelated-addressed micro-LED arrays on printed circuit board for display and communication applications," IEEE J. Electron Devices Soc. **5**, 90–94 (2017).
11. R. P. Green, J. J. D. McKendry, D. Massoubre, E. Gu, M. D. Dawson, and A. E. Kelly, "Modulation bandwidth studies of recombination processes in blue and green InGaN quantum well micro-light-emitting diodes," Appl. Phys. Lett. **102**, 091103 (2013).

12. M. S. Islim, R. X. Ferreira, X. He, E. Xie, S. Videv, S. Viola, S. Watson, N. Bamiedakis, R. V. Penty, I. H. White, A. E. Kelly, E. Gu, H. Haas, and M. D. Dawson, "Towards 10 Gb/s orthogonal frequency division multiplexing-based visible light communication using a GaN violet micro-LED," Photon. Res. **5**, A35–A43 (2017).
13. S. Zhu, P. Qiu, Z. Qian, X. Shan, Z. Wang, K. Jiang, X. Sun, X. Cui, G. Zhang, D. Li, and P. Tian, "2 Gbps free-space ultraviolet-C communication based on a high-bandwidth micro-LED achieved with pre-equalization," Opt. Lett. **46**, 2147–2150 (2021).
14. C. Jeon, H. W. Choi, E. Gu, M. D. Dawson, and S. Member, "High-density matrix-addressable AlInGaN-based 368-nm microarray light-emitting diodes," IEEE Photon. Technol. Lett. **16**, 2421–2423 (2004).
15. B. Guilhabert, D. Massoubre, E. Richardson, J. J. D. McKendry, G. Valentine, R. K. Henderson, I. M. Watson, E. Gu, and M. D. Dawson, "Sub-micron lithography using InGaN micro-LEDs: mask-free fabrication of LED arrays," IEEE Photon. Technol. Lett. **24**, 2221–2224 (2012).
16. X. He, E. Xie, M. S. Islim, A. A. Purwita, J. J. D. McKendry, E. Gu, H. Haas, and M. D. Dawson, "1 Gbps free-space deep-ultraviolet communications based on III-nitride micro-LEDs emitting at 262 nm," Photon. Res. **7**, B41–B47 (2019).
17. R. X. G. Ferreira, E. Xie, J. J. D. McKendry, S. Rajbhandari, H. Chun, G. Faulkner, S. Watson, A. E. Kelly, and E. Gu, "High bandwidth GaN-based micro-LEDs for multi-Gb/s visible light communications," IEEE Photon. Technol. Lett. **28**, 2023–2026 (2016).
18. H. Amano, R. Collazo, C. D. Santi, S. Einfeldt, M. Funato, J. Glaab, S. Hagedorn, A. Hirano, H. Hirayama, R. Ishii, Y. Kashima, R. Kirste, M. Kneissl, R. W. Martin, F. Mehnke, M. Meneghini, A. Ougazzaden, P. Parbrook, S. Rajan, and P. Reddy, "The 2020 UV emitter roadmap," J. Phys. D **53**, 503001 (2020).
19. M. Kneissl, T. Y. Seong, J. Han, and H. Amano, "The emergence and prospects of deep-ultraviolet light-emitting diode technologies," Nat. Photonics **13**, 233–244 (2019).
20. S. W. H. Chen, Y.-M. Huang, Y.-H. Chang, Y. Lin, F.-J. Liou, Y.-C. Hsu, J. Song, J. Choi, C.-W. Chow, C.-C. Lin, R.-H. Horng, Z. Chen, J. Han, T. Wu, and H.-C. Kuo, "High-bandwidth green semipolar (20-21) InGaN/GaN micro light-emitting diodes for visible light communication," ACS Photon. **7**, 2228–2235 (2020).
21. D. Tsonev, H. Chun, S. Rajbhandari, J. J. D. McKendry, S. Videv, E. Gu, and M. Haji, "A 3-Gb/s single-LED OFDM-based wireless VLC link using a gallium nitride μLED," IEEE Photon. Technol. Lett. **26**, 637–640 (2014).
22. J. F. C. Carreira, E. Xie, R. Bian, J. Herrnsdorf, H. Haas, E. Gu, M. J. Strain, and M. D. Dawson, "Gigabit per second visible light communication based on AlGaInP red micro-LED micro-transfer printed onto diamond and glass," Opt. Express **28**, 12149–12156 (2020).
23. H. Ding, G. Chen, A. K. Majumdar, B. M. Sadler, and Z. Xu, "Modeling of non-line-of-sight ultraviolet scattering channels for communication," IEEE J. Sel. Areas Commun. **27**, 1535–1544 (2009).
24. X. Liu, Z. Wei, M. Li, L. Wang, Z. Liu, C. Yu, L. Wang, Y. Luo, and H. Y. Fu, "Experimental investigation of 16.6 Gbps SDM-WDM visible light communication based on a neural network receiver and tricolor mini-LEDs," Opt. Lett. **46**, 2888–2891 (2021).
25. G. Cossu, A. M. Khalid, P. Choudhury, R. Corsini, and E. Ciaramella, "3.4 Gbit/s visible optical wireless transmission based on RGB LED," Optics Express **20**, B501–B506 (2012).
26. X. Sun, Z. Zhang, A. Chaaban, T. K. Ng, C. Shen, R. Chen, J. Yan, H. Sun, X. Li, J. Wang, J. Li, M.-S. Alouini, and B. S. Ooi, "71-Mbit/s ultraviolet-B LED communication link based on 8-QAM-OFDM modulation," Opt. Express **25**, 23267–23274 (2017).
27. https://doi.org/10.15129/1899e15a-2d46-4e80-9d3f-93f3b66abeb7.